Japanese Journal of Applied Physics

The Japan Society of Applied Physics

RAPID COMMUNICATION

Improvement of dynamic range and repeatability in a refractive-index-sensing optical comb by combining saturable-absorber-mirror mode-locking with an intracavity multimode interference fiber sensor

To cite this article: Ryo Oe *et al* 2019 *Jpn. J. Appl. Phys.* **58** 060912

View the article online for updates and enhancements.

This content was downloaded from IP address 150.59.28.18 on 15/06/2019 at 02:49

Japanese Journal of Applied Physics **58**, 060912 (2019) **RAPID COMMUNICATION**
https://doi.org/10.7567/1347-4065/ab219a

Improvement of dynamic range and repeatability in a refractive-index-sensing optical comb by combining saturable-absorber-mirror mode-locking with an intracavity multimode interference fiber sensor

Ryo Oe[1,2], Takeo Minamikawa[2,3,4], Shuji Taue[5], Takuya Nakahara[1], Hidenori Koresawa[1,2], Takahiko Mizuno[2,3,4], Masatomo Yamagiwa[2,3,4], Yasuhiro Mizutani[2,6], Hirotsugu Yamamoto[2,7], Tetsuo Iwata[2,4], Yoshiaki Nakajima[2,8], Kaoru Minoshima[2,3,8], and Takeshi Yasui[2,3,4*]

[1]*Graduate School of Advanced Technology and Science, Tokushima University, Tokushima, Tokushima 770-8506, Japan*
[2]*JST, ERATO, MINOSHIMA Intelligent Optical Synthesizer Project, Tokushima, Tokushima 770-8506, Japan*
[3]*Institute of Post-LED Photonics (pLED), Tokushima University, Tokushima, Tokushima 770-8506, Japan*
[4]*Graduate School of Technology, Industrial and Social Sciences, Tokushima University, Tokushima, Tokushima 770-8506, Japan*
[5]*School of System Engineering, Kochi University of Technology, Kami, Kochi 782-8502, Japan*
[6]*Graduate School of Engineering, Osaka University, Suita, Osaka 565-0871, Japan*
[7]*Center for Optical Research and Education, Utsunomiya University, Utsunomiya, Tochigi 321-8585, Japan*
[8]*Graduate School of Informatics and Engineering, The University of Electro-Communications, Chofu, Tokyo 182-8585, Japan*

*E-mail: yasui.takeshi@tokushima-u.ac.jp

Received April 20, 2019; revised May 6, 2019; accepted May 13, 2019; published online May 31, 2019

A mode-locked fiber comb equipped with a multimode interference fiber sensor functions as a high-precision refractive-index (RI) sensor benefitting from precise RF measurement. However, its dynamic range and repeatability are hampered by the inherent characteristics of nonlinear-polarization-rotation mode-locking oscillation. In this article, we introduce saturable-absorber-mirror mode-locking for RI sensing with a wide dynamic range and high repeatability. While the RI dynamic range was expanded to 41.4 dB due to high robustness against cavity disturbance, the self-starting capability without the need for polarization control improves the RI sensing repeatability to 1.10×10^{-8} for each mode-locking activation. The improved dynamic range and repeatability will be useful for enhancing the performance of RI sensing.
© 2019 The Japan Society of Applied Physics

The refractive-index (RI) is an important physical value of materials. Therefore, RI sensing has been widely used for the identification or characterization of materials. Among various RI sensors, the RI fiber sensor benefits from compactness, simplicity, flexibility, robustness against noise and availability in various environments; hence, this sensor has been used for various applications, including ethanol sensing,[1)] glucose sensing,[2)] biosensing,[3)] and gas sensing.[4)] In most cases, a change in the RI of the sample is converted into a shift of optical spectrum via the surface plasmon resonance[5–8)] or the multimode interference (MMI).[9–11)] However, the precision of RI sensing is limited by the sharpness of the maximum or minimum of the optical spectrum as well as by the instrumentational resolution.

If a change in the RI of a sample is transformed into a photonic RF signal in combination with a sharpened spectrum, the RI sensing benefits from high-precision, high functionality, convenience, and low cost by making use of frequency standards and precise measurement apparatuses in the RF region. Such photonic RF fiber sensors have been effectively applied for strain sensing[12)] and ultrasound sensing[13,14)] by using multiple-longitudinal-mode or multiple-polarization-mode spacing in a continuous-wave (CW) fiber laser or a CW fiber-Bragg-grating laser. However, the inherent frequency fluctuation of mode spacing hampers high-precision RI sensing.

Recently, an optical frequency comb (OFC) appeared as a new photonic RF fiber sensor for determining liquid RI[15)] as well as for strain,[16)] acoustic wave,[17)] and ultrasound sensing.[18)] Although OFC has been widely used as an optical frequency ruler secured by a frequency standard,[19–21)] the OFC was used here as a photonic RF converter, converting the sample RI into an OFC mode spacing f_{rep} via a combination of RI-dependent tunable bandpass filtering by an intracavity MMI fiber sensor and wavelength dispersion by a cavity fiber. Due to the ultranarrow linewidth and high stability in the mode-locking oscillation, this MMI-OFC enables us to precisely measure the RI-dependent f_{rep} shift by using an RF frequency counter synchronized with a rubidium frequency standard, leading to an RI resolution of 4.9×10^{-6} refractive-index units (RIU) and an RI accuracy of 5.4×10^{-5} RIU.

Notable problems with the previous MMI-OFC include its limited dynamic range and the low repeatability of RI sensing, which are caused by the nonlinear-polarization rotation (NPR)[22)] used for mode-locking oscillation in the MMI-OFC. Although NPR has been widely used for the fiber-based optical comb with broad optical bandwidth, it is less robust against external disturbance to the cavity because of high sensitivity to the fiber birefringence. In the MMI-OFC, a large change in the sample RI causes a change in the intracavity polarization condition via the intracavity MMI fiber sensor, leading to a nonnegligible disturbance to the cavity and the disruption of mode-locking oscillation. This is the reason for the limited dynamic range of RI sensing. On the other hand, NPR-based mode-locking oscillation is activated by polarization adjustment in the fiber cavity with a polarization controller. While such polarization adjustment enables flexible mode-locking oscillation, f_{rep} changes with every mode-locking activation, leading to low repeatability. If high repeatability of f_{rep} can be achieved in an RI sensing MMI-OFC, the RI sensing repeatability will be enhanced.

To overcome the limited dynamic range and the low repeatability of RI sensing, a robust mode-locking mechanism with fewer degrees of freedom is required in the RI sensing MMI-OFC. One possible candidate for such a purpose is mode-locking oscillation with a saturable-absorber mirror (SAM).[23)] SAM enables easy, stable, and robust mode-locking oscillation without the need for polarization control. While such characteristics in SAM enable us to

 © 2019 The Japan Society of Applied Physics

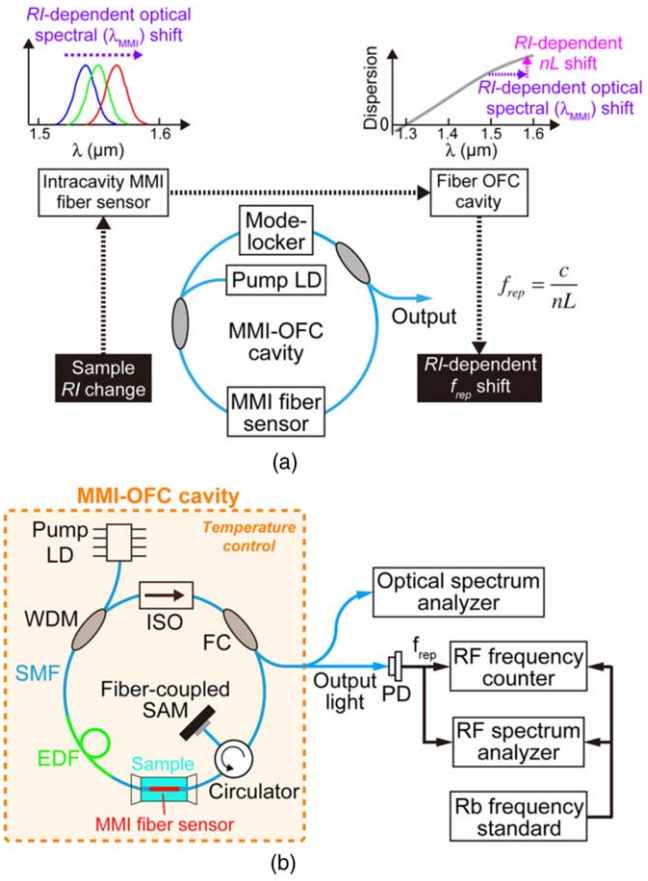

Fig. 1. (Color online) (a) Principle of operation for MMI-OFC. (b) Experimental setup of SAM-MMI-OFC. Pump LD, pumping laser diode; WDM, wavelength-division-multiplexing coupler; SMF, single-mode fiber; EDF, erbium-doped fiber; SAM module, saturable absorbed mirror module; ISO, polarization-insensitive isolator; FC, 70:30 fiber coupler; PD, photodiode.

expand the dynamic range of RI sensing in MMI-OFC, mode-locking oscillation with fewer degrees of freedom will contribute to obtaining high repeatability for both f_{rep} and RI sensing. In this article, we evaluate the validity of SAM-based MMI-OFC (SAM-MMI-OFC) by comparing it with the previous NPR-based MMI-OFC (NPR-MMI-OFC).

Figure 1(a) shows the principle of operation for a MMI-OFC.[15] The MMI-OFC has a ring-type fiber cavity containing a mode-locker and a MMI fiber sensor. The intracavity of the MMI fiber sensor functions as an RI-dependent tunable optical bandpass filter (bandpass center wavelength $= \lambda_{MMI}$) via the MMI and the Goos–Hänchen shift on the surface of the MMI fiber sensor. In other words, the intracavity MMI fiber sensor shifts the optical spectrum (λ_{MMI}) of the MMI-OFC depending on the sample RI. The wavelength-shifted MMI-OFC spectrum experiences the wavelength dispersion of the cavity fiber, resulting in the conversion from the RI-dependent optical spectral shift to an RI-dependent shift in the optical cavity length nL. Since f_{rep} of OFC is given by c/nL, where c is the velocity of light in a vacuum, a change in the RI of a sample can be read out as an RI-dependent f_{rep} shift (Δf_{rep}).

We modified a mode-locked Er:fiber laser oscillator for the SAM-MMI-OFC, as shown in Fig. 1(b). This oscillator had a ring cavity, including a 3.3 m length of single-mode fiber (SMF, SMF-28, Corning, dispersion at 1550 nm $= 17\ \mathrm{ps\,km^{-1}\,nm^{-1}}$), a 0.5 m length of erbium-doped fiber (ER80-4/125, LIEKKI, dispersion at 1550 nm $= -65\ \mathrm{ps\,km^{-1}\,nm^{-1}}$), a fiber-coupled saturable absorbed mirror (FC-SAM, SAM-1550-4-4ps-FC, BATOP, high reflection band = 1480–1580 nm, absorbance = 4%, modulation depth = 2.4%, relaxation time constant ~4 ps, mounted on a 1 m SMF cable with FC connector), a polarization-insensitive isolator (ISO, PSSI-55-P-I-N-B-I, AFR), a 70:30 fiber coupler (FC, SBC-1-55-30-1-B-1, AFR), a wavelength-division-multiplexing coupler (WDM, WDM-1-9855-1-L-1-F, AFR), a pumping laser diode (BL976-PAG900, Thorlabs, wavelength = 980 nm, power = 900 mW), a fiber circulator (FCIR-55-1-B-1-1, AFR), and an intracavity MMI fiber sensor. The intracavity MMI fiber sensor was composed of a clad-less MMF (FG125LA, Thorlabs, core diameter = 125 μm, fiber length = 58 mm) with a pair of SMFs at both ends (core diameter = 6 μm, clad diameter = 125 μm, fiber length = 54 mm), the detail of which is given elsewhere.[15] Here, we set m to 4 for the use of the intracavity MMI fiber sensor as the RI-dependent tunable bandpass filter. The SAM functions as a stable mode-locker via a fiber circulator. The fiber cavity was enclosed in an aluminum box, and its temperature was controlled to 26.0 °C by a combination of a Peltier heater (TEC1-12708, Kaito Denshi, power = 76 W), a thermistor (PB7-42H-K1, Yamaki) and a temperature controller (TED200, Thorlabs, PID control) [not shown in Fig. 1(b)]. The output light from the oscillator was detected by a photodetector, and f_{rep} was measured by an RF frequency counter (53 230 A, Keysight Technologies, frequency resolution = 12 digit $\mathrm{s^{-1}}$) and an RF spectrum analyzer (E4402B, Keysight Technologies, frequency resolution = 1 Hz), both of which were synchronized to a rubidium frequency standard (FS725, Stanford Research Systems, accuracy $= 5 \times 10^{-11}$ and instability $= 2 \times 10^{-11}$ at 1 s). Additionally, its optical spectrum was measured by an optical spectrum analyzer (AQ6315A, Yokogawa Electric Corp., wavelength accuracy = 0.02 nm, wavelength resolution = 0.02 nm). For comparison, we prepared the NPR-MMI-OFC[15] and enclosed it in the same temperature-controlled box. The specification of the NPR-MMI-OFC was set to be similar to the SAM-MMI-OFC, as shown later. The same MMI fiber sensor was used in the NPR-MMI-OFC.

Before evaluating the performance of RI sensing, we compared an optical spectrum and an RF spectrum between the SAM-MMI-OFC and NPR-MMI-OFC. Pure water was used here as a liquid sample. The red and blue plots in Fig. 2(a) show an optical spectrum of the SAM-MMI-OFC (center wavelength = 1558.8 nm, spectral bandwidth = 0.8 nm, mean power = 1.43 mW) and the NPR-MMI-OFC (center wavelength = 1552.2 nm, spectral bandwidth = 7.7 nm, mean power = 1.46 mW), respectively. The soliton mode-locking oscillation was achieved near the zero-dispersion region of the cavity ($-0.0338\ \mathrm{ps^2}$ for the SAM-MMI-OFC and $-0.0339\ \mathrm{ps^2}$ for the NPR-MMI-OFC). The spectral bandwidth in the SAM-MMI-OFC was significantly narrower than that in the NPR-MMI-OFC. While the SAM-MMI-OFC can be easily mode-locked by the narrower spectral light and, hence, by the longer pulse light, the mode-locking oscillation of the NPR-MMI-OFC needs the broader spectral light and the shorter pulse light together with precise polarization control. Such ease of mode-locking oscillation in the SAM-MMI-OFC

© 2019 The Japan Society of Applied Physics

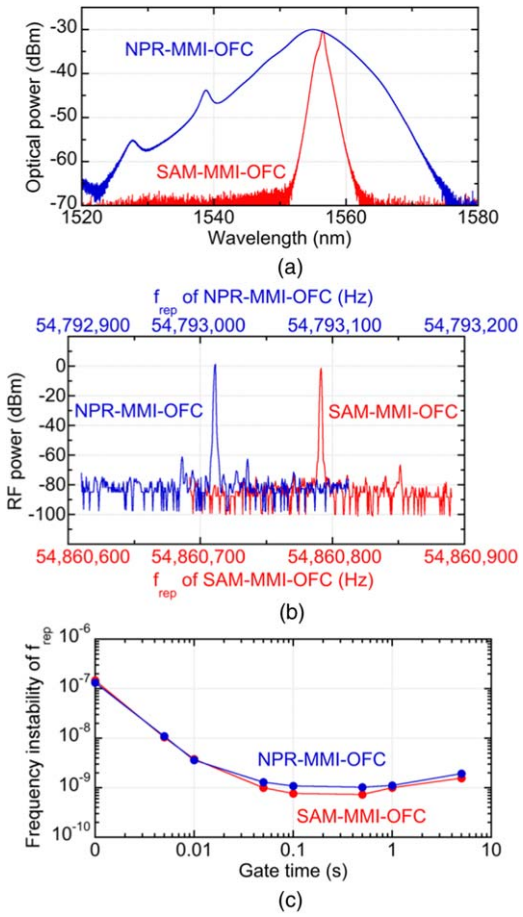

Fig. 2. (Color online) Comparison of (a) optical spectrum, (b) RF spectrum of f_{rep}, and (c) frequency instability of f_{rep} between SAM-MMI-OFC and NPR-MMI-OFC.

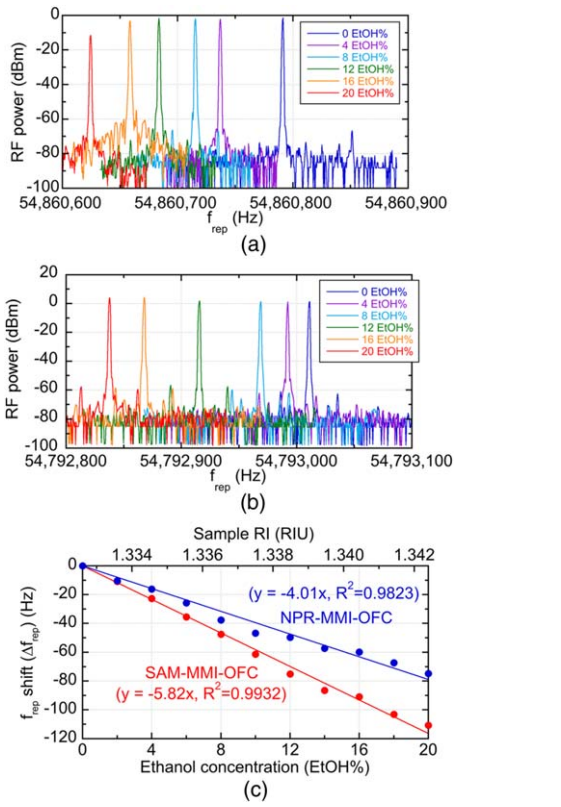

Fig. 3. (Color online) RI-dependent f_{rep} shift in (a) SAM-MMI-OFC and (b) NPR-MMI-OFC. (c) Relation between ethanol concentration or sample RI and f_{rep} shift (Δf_{rep}) in SAM-MMI-OFC (red plot) and NPR-MMI-OFC (blue plot).

will contribute to the robustness against the cavity disturbance caused by the intracavity MMI fiber sensor. Figure 2(b) compares the RF spectrum of f_{rep} between the SAM-MMI-OFC (red plot) and the NPR-MMI-OFC (blue plot). f_{rep} was 54.86 MHz for the SAM-MMI-OFC and 54.79 MHz for the NPR-MMI-OFC, which are approximately equal. Both RF spectra have a similar linewidth of approximately 1 Hz, which is limited by the instrumentational resolution of the RF spectrum analyzer rather than the actual RF spectrum of f_{rep}. We also compare the frequency instability of f_{rep} between the SAM-MMI-OFC and the NPR-MMI-OFC. The red and blue plots in Fig. 2(c) show the frequency instabilities of f_{rep} with respect to the gate time, which is defined as the ratio of the f_{rep} fluctuation to the mean f_{rep} value. Little difference was observed between them; in other words, the use of SAM in MMI-OFC does not degrade the f_{rep} instability and has the potential to achieve the same RI resolution as the NPR-MMI-OFC.

To confirm the RI sensing capability in the optical region, we first investigated the RI-dependent λ_{MMI} shift in the SAM-MMI-OFC and the NPR-MMI-OFC. Mixtures of ethanol and pure water were used here as liquid samples. The sample RI was adjusted by changing the ethanol and water mixture ratio. Furthermore, the temperature of the sample was controlled at 22 °C by a combination of a K-type thermocouple (TJA-550K, AS ONE), a cord heater (603-60-69-01, Tokyo Glass Kikai, power = 15 W), and a temperature controller (TJA-550, AS ONE, PID control, display resolution = 0.1 °C). The relationship between the ethanol volume concentration EC (unit: EtOH%) and the sample RI (unit: RIU) is given by $\mathrm{RI} = 1.3326 + 4.90 \times 10^{-4} \times \mathrm{EC}$.[24] The resulting RI-dependent λ_{MMI} shift was determined to be 94.5 nm/RIU for the SAM-MMI-OFC and 67.8 nm/RIU for NPR-MMI-OFC, respectively (not shown). We next evaluated the relation between the sample RI and the f_{rep} shift (Δf_{rep}) in the SAM-MMI-OFC and NPR-MMI-OFC. Figures 3(a) and 3(b) respectively show the RI-dependent RF spectrum shift of f_{rep} obtained by the SAM-MMI-OFC and the NPR-MMI-OFC for the ethanol/water samples with different mixture ratios (=0–20 EtOH%, corresponding to 1.333–1.342 RIU) and acquired by an RF spectrum analyzer. The magnitude of the spectral shift was significantly larger than that of the spectral linewidth in both. Then, we measured the RI-dependent Δf_{rep} more precisely by using an RF frequency counter, as shown in Fig. 3(c). Although the linear relation was confirmed in the SAM-MMI-OFC and the NPR-MMI-OFC, the former shows better linearity than the latter. The RF slope coefficient was determined to be −5.82 Hz/EtOH% for the SAM-MMI-OFC and −4.01 Hz/EtOH% for the NPR-MMI-OFC. The RF slope coefficient ratio [= (−5.82 Hz/EtOH%)/(−4.01 Hz/EtOH%) = 1.45] significantly agrees with the optical slope coefficient ratio of the SAM-MMI-OFC to the NPR-MMI-OFC [= (94.5 nm/RIU)/(67.8 nm/RIU) = 1.39]; the difference in the RF slope coefficient between the SAM-MMI-OFC and the NPR-MMI-OFC is mainly due to the difference in the optical slope coefficient between the two. From these slope coefficients and the frequency fluctuation of f_{rep}, the RI resolution was

© 2019 The Japan Society of Applied Physics

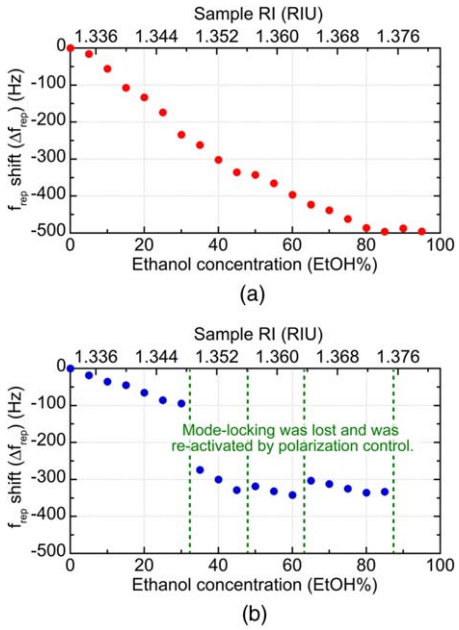

Fig. 4. (Color online) Relation between ethanol concentration or sample RI and f_{rep} shift (Δf_{rep}) in (a) SAM-MMI-OFC and (b) NPR-MMI-OFC.

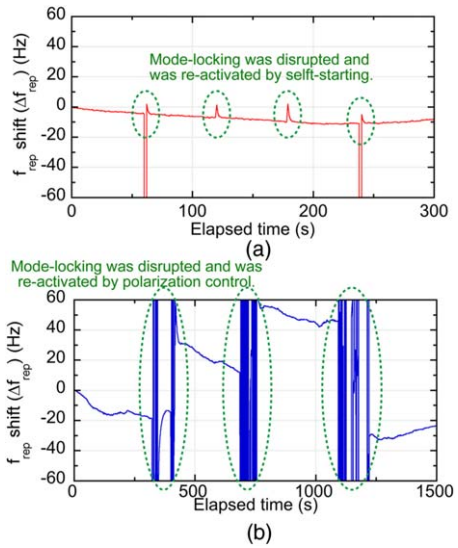

Fig. 5. (Color online) Temporal change in f_{rep} when the mode-locking oscillation was disrupted. (a) SAM-MMI-OFC and (b) NPR-MMI-OFC.

determined to be 3.37×10^{-6} for the SAM-MMI-OFC and 6.92×10^{-6} for the NPR-MMI-OFC at a measurement time of 0.5 s.

We further investigated the RI-dependent Δf_{rep} of water/ethanol samples within a wider range of mixture ratio (0−100 EtOH%, corresponding to 1.333–1.382 RIU). Figure 4(a) shows the RI-dependent Δf_{rep} of the water/ethanol sample in the SAM-MMI-OFC. The SAM-based mode-locking oscillation was maintained in all ethanol concentrations. The resulting slope coefficient at the lower concentrations was larger than that at the higher concentrations because the RI value of the water/ethanol mixture increased from the low concentration (= 0−80 EtOH%), reached a plateau approximately 80%, and decreased in the higher concentrations (= 80−100 EtOH%).[11] Figure 4(b) shows the RI-dependent Δf_{rep} of the water/ethanol sample in the NPR-MMI-OFC. In contrast to the SAM-MMI-OFC, the NPR-based mode-locking oscillation was lost four times due to the lower robustness against the cavity disturbance caused by the intracavity MMI fiber sensor. When we activated the mode-locking oscillation again by fine adjustment of an intracavity polarization controller, the f_{rep} value significantly jumped from the f_{rep} value before the mode-locking oscillation was lost. As a result, the RI-dependent Δf_{rep} slope shows several discontinuity points. Such discontinuity points hamper the wide dynamic range of RI sensing in the NPR-MMI-OFC. The dynamic range of RI sensing in the SAM-MMI-OFC and the NPR-MMI-OFC is given by

$$\begin{aligned} DR_{SAM} &= 10 \log [(RI_{max} - RI_{min}) / (RI\ resolution)] \\ &= 10 \log [(1.3792–1.3326) / (3.37 \times 10^{-6})] \\ &= 41.4 dB, \end{aligned} \quad (1)$$

$$\begin{aligned} DR_{NPR} &= 10 \log [(1.3473 – 1.3326) / (6.92 \times 10^{-6})] \\ &= 33.3 dB, \end{aligned} \quad (2)$$

where RI_{max} and RI_{min} are the maximum and minimum RI values. This comparison clearly indicates the superiority of the SAM-MMI-OFC over the NPR-MMI-OFC for a wide dynamic range of RI sensing. The maximum RI will be limited by the RI of the clad-less MMF (= 1.444 RIU) because the MMI fiber sensor is based on the total reflection at a boundary between the clad-less MMF surface and the sample.

We evaluated the repeatability of f_{rep} in the SAM-MMI-OFC and the NPR-MMI-OFC. Figure 5(a) shows the temporal change of f_{rep} in the SAM-MMI-OFC when the mode-locking oscillation was disrupted by turning the pumping LD off. Due to the self-starting of the mode-locking oscillation without the need for additional adjustment of the intracavity component, the f_{rep} values were recovered with high repeatability before and after the disruption. The slow temporal change of f_{rep} was mainly due to the residual thermal drift of nL. However, the temporal behavior of f_{rep} was almost continuous even though the mode-locking oscillation was disrupted. Frequency deviation before and after disruption of the mode-locking oscillation was 0.60 ± 0.66 Hz for 4 disruptions, corresponding to a repeatability of $(1.10 \pm 1.21) \times 10^{-8}$ in f_{rep}. This repeatability of f_{rep} is equivalent to the repeatability of the RI measurement. On the other hand, with the NPR-MMI-OFC, it is difficult to activate the mode-locking oscillation as self-starting when the mode-locking oscillation is disrupted by turning the pumping LD off. The NPR-MMI-OFC needs the precise adjustment of the polarization controller for the activation of the mode-locking oscillation. As a result, f_{rep} increased by several tens of Hz at every disruption point, even though the scale of the polarization controller was set to that before the disruption, as shown in Fig. 5(b). Frequency deviation before and after disruption of the mode-locking oscillation was 46.0 ± 4.67 Hz for 3 disruptions, corresponding to the f_{rep} repeatability of $(8.40 \pm 0.85) \times 10^{-7}$. Thus, the SAM-MMI-OFC has better f_{rep} repeatability f than the NPR-MMI-OFC.

We here discuss the possibility of the absolute measurement of the sample RI based on one-to-one correspondence between the sample RI and f_{rep}. In the previous research on MMI-OFC,[15] the low repeatability of f_{rep} in the NPR-MMI-OFC [see Fig. 5(b)] hampers such an absolute RI

© 2019 The Japan Society of Applied Physics

measurement. Therefore, the relative measurement was performed based on a one-to-one correspondence between the sample RI and the f_{rep} shift (Δf_{rep}). The use of SAM in MMI-OFC benefits from the high repeatability of f_{rep} [see Fig. 5(a)] in addition to the wide dynamic range of RI sensing. However, a slow temporal change of f_{rep} remained due to the residual thermal drift of nL, even though the temperature control of the fiber cavity was activated. This remaining change is the last barrier preventing the absolute measurement of the sample RI. One possible method to get rid of this barrier is to compensate the drifted f_{rep} by another measured parameter (for example, the carrier-envelope-offset frequency of OFC, optical power, optical spectrum, and so on) related to the thermal condition of the fiber cavity. Currently, work is in progress to achieve the absolute measurement of the sample RI based on a one-to-one correspondence between the sample RI and f_{rep}.

In summary, we proposed the use of SAM-based mode-locking, in place of NPR-based mode-locking, in MMI-OFCs. An improved dynamic range and repeatability were effectively demonstrated in RI sensing of the ethanol/water sample. While the RI dynamic range was significantly increased due to the high robustness against the cavity disturbance caused by the MMI fiber sensor, the self-starting capability without the need for polarization control significantly improves the repeatability of f_{rep}-based RI sensing at every mode-locking activation. RI sensing based on SAM-MMI-OFC will be a powerful tool for the quality control of liquid products, biosensing, and gas sensing.

Acknowledgments This work is supported by Exploratory Research for Advanced Technology (ERATO, MINOSHIMA Intelligent Optical Synthesizer Project, JPMJER1304) from Japanese Science and Technology Agency and Grant-in-Aid for Exploratory Research (19H00871) from the Japan Society for the Promotion of Science.

ORCID iDs Takeo Minamikawa https://orcid.org/0000-0003-3528-7163 Kaoru Minoshima https://orcid.org/0000-0003-1301-1406 Takeshi Yasui https://orcid.org/0000-0001-7742-6155

1) S. K. Srivastava, R. Verma, and B. D. Gupta, Sens. Actuators B **153**, 194 (2011).
2) S. Binu, V. P. Mahadevan Pillai, V. Pradeepkumar, B. B. Padhy, C. S. Joseph, and N. Chandrasekaran, Mater. Sci. Technol. C **29**, 183 (2009).
3) H. Tazawa, T. Kanie, and M. Katayama, Appl. Phys. Lett. **91**, 113901 (2007).
4) S. Sekimoto, H. Nakagawa, S. Okazaki, K. Fukuda, S. Asakura, T. Shigemori, and S. Takahashi, Sens. Actuators B **66**, 142 (2000).
5) W. B. Lin, J. M. Chovelon, and N. Jaffrezic-Renault, Appl. Opt. **39**, 3261 (2000).
6) P. Bhatia and B. D. Gupta, Plasmonics **8**, 779 (2013).
7) K. Balaa, M. Kanso, S. Cuenot, T. Minea, and G. Louarn, Sens. Actuators B **126**, 198 (2007).
8) J. F. Masson, Y. C. Kim, L. A. Obando, W. Peng, and K. S. Booksh, Appl. Spectrosc. **60**, 1241 (2006).
9) Y. Jung, S. Kim, D. Lee, and K. Oh, Meas. Sci. Technol. **17**, 1129 (2006).
10) Q. Wang and G. Farrell, Opt. Lett. **31**, 317 (2006).
11) S. Taue, Y. Matsumoto, H. Fukano, and K. Tsuruta, Jpn. J. Appl. Phys. **51**, 04DG14 (2012).
12) S. Liu, Z. Yin, L. Zhang, L. Gao, X. Chen, and J. Cheng, Opt. Lett. **35**, 835 (2010).
13) T. Guo, A. C. Wong, W. S. Liu, B. O. Guan, C. Lu, and H. Y. Tam, Opt. Express **19**, 2485 (2011).
14) Y. Liang, L. Jin, L. Wang, X. Bai, L. Cheng, and B.-O. Guan, Sci. Rep. **7**, 40849 (2017).
15) R. Oe et al., Opt. Express **26**, 19694 (2018).
16) T. Minamikawa, T. Ogura, Y. Nakajima, E. Hase, Y. Mizutani, H. Yamamoto, K. Minoshima, and T. Yasui, Opt. Express **26**, 9484 (2018).
17) S. Wang, P. Lu, H. Liao, L. Zhang, D. Liu, and J. Zhang, J. Mod. Opt. **60**, 1892 (2013).
18) T. Minamikawa et al., OSA Continuum **2**, 439 (2019).
19) T. Udem, J. Reichert, R. Holzwarth, and T. W. Hänsch, Opt. Lett. **24**, 881 (1999).
20) M. Niering et al., Phys. Rev. Lett. **84**, 5496 (2000).
21) T. Udem, R. Holzwarth, and T. W. Hänsch, Nature **416**, 233 (2002).
22) A. Komarov, H. Leblond, and F. Sanchez, Phys. Rev. A **72**, 063811 (2005).
23) B. Ortaç, M. Plötner, J. Limpert, and A. Tünnermann, Opt. Express **15**, 16794 (2007).
24) J. V. Herráez and R. Belda, J. Solution Chem. **35**, 1315 (2006).

© 2019 The Japan Society of Applied Physics